

Stability of Hierarchical Gyroid Structures in Frustrated ABC Triblock Copolymers

Xintong You, Meijiao Liu, Qingshu Dong,* and Weihua Li*



Cite This: *Macromolecules* 2023, 56, 8157–8167



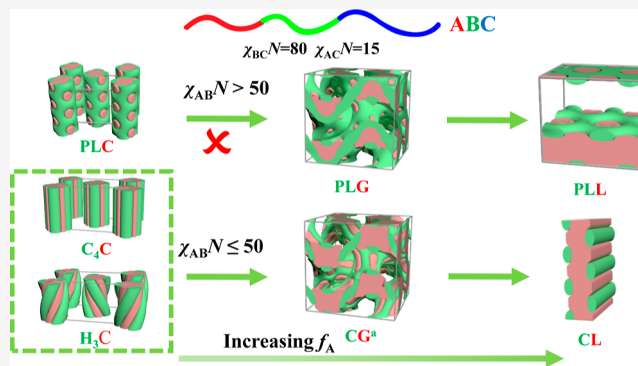
Read Online

ACCESS |

Metrics & More

Article Recommendations

ABSTRACT: Linear ABC triblock copolymer with a repulsive interaction between A and C blocks significantly weaker than those between the other two pairs of adjacent blocks can self-assemble into various hierarchical structures composed of discrete B-subdomains sitting on A/C interfaces. However, whether the hierarchical structures still follow the common transition sequence of sphere → cylinder → gyroid → lamella remains an interesting question to be answered. In this work, the self-assembly of frustrated linear ABC triblock copolymers is investigated using self-consistent field theory, focusing on the formation of different hierarchical gyroid structures. Our results show that hierarchical gyroid structures are not commonly formed between hierarchical cylindrical and lamellar structures in the case of $\chi_{AB}N = \chi_{BC}N = 80 \gg \chi_{AC}N = 15$. The stability regions of various gyroid phases appear and expand as $\chi_{AB}N$ is gradually decreased. We speculate that the absence of hierarchical gyroid structures is mainly induced by the increased constraint on the configurations due to the highly nonuniform distribution of discrete B-subdomains on the irregular A/C interface of gyroid. As $\chi_{AB}N$ decreases, the A/B interface widens and B-subdomains move into main A-domain, relieving the constraint on the A/B junction point and thus on the configuration of A-block. In a word, our work shows that the substructure of the hierarchical structures imposes a nontrivial effect on the relative stability of various hierarchical structures, which may disrupt the common transition sequence in a frustrated linear ABC triblock copolymer.



INTRODUCTION

Block copolymer has been attracting abiding interest due to its unique ability of self-assembling into various ordered nanostructures that exhibit promising applications in a wide range of fields.^{1–8} AB diblock copolymer, as the simplest block copolymer, has been intensively studied experimentally and theoretically, and thus its self-assembly behavior has been well understood.⁹ In particular, self-consistent field theory (SCFT), which can accurately calculate the free energy of each ordered phase and has been proven as one of the most powerful methods for the study of block copolymers, has verified that the AB diblock copolymer exhibits a phase sequence mainly consisting of lamella (L), hexagonally arranged cylinders (C_6), bicontinuous double-gyroid (G) network, and a body-centered cubic (BCC) lattice of spheres, as its volume fraction of one block changes from symmetric to asymmetric.^{10–13} The appearance of the G phase has received extensive attention because its bicontinuous feature makes it become a promising candidate for the fabrication of many functional materials.^{14–20} This transition sequence as well as the self-assembly mechanism of the AB diblock has laid the foundation for understanding the self-assembly behaviors of other block copolymers with more complex architectures.

Indeed, the transitions of $L \rightarrow G \rightarrow C_6 \rightarrow BCC$ are induced by the tapering interaction energy and increasing entropic contribution. On the other hand, the effect of spontaneous interfacial curvature increases as the composition becomes increasingly asymmetric, which can also be utilized to rationalize the common transition sequence. Reasonably, the compositional effect on the phase transitions should be robust for many different block copolymers. SCFT results have demonstrated that many chain architectures of AB-type block copolymers do not change the common phase sequence, but shift the phase boundaries.²¹ Moreover, the compositional effect can also be used to interpret the phase transitions in some ABC-type block copolymers.^{22–38} From the aspect of the compositional effect on the domain geometry, the symmetric ABC linear triblock copolymer exhibits a similar transition

Received: June 26, 2023

Revised: September 25, 2023

Published: October 13, 2023



sequence from lamella to double-gyroid, cylinder, and sphere. The difference lies in the alternate arrangement of A and C domains, e.g., the two separate networks of the double-gyroid phase are composed of A and C blocks, respectively. Exceptionally, for the cylindrical phase, the alternate arrangement alters the packing lattice from hexagonal to tetragonal, leading to the formation of a tetragonal array of alternate A and C cylinders (C_4).^{24,25} Nevertheless, the alternating double-gyroid phase still commonly appears between the lamella and cylinder phases.³⁹

However, some recent SCFT studies predict the absence of the G phase in the transition sequence with respect to the composition for some AB-type as well as ABC-type block copolymers. These theoretical works further reveal that the effects causing the disappearance of the G phase in the two categories of systems are different.^{40,41} In AB-type block copolymers, it is well-known that the architectural asymmetry can deflect phase boundaries. A typical AB-type of asymmetric architecture is AB_n miktoarm star copolymer,^{42–44} in the phase diagram of which the phase boundaries are deflected to large volume fraction of A-block (f). In other words, the phase region of the G phase with A-channels (G_A) is expanded, while that of B-channels (G_B) is narrowed. Though the narrowing degree of the G_B phase region can be raised by increasing n , it would not disappear due to the limited effect of the AB_n architecture. Very recently, Li and co-workers have proposed that the deflection of the phase boundaries can be largely amplified by tailoring the architecture of A-blocks to form a radial distribution, leading to the disappearance of the G phase at the compressed side of the phase diagram.^{41,44} In ABC-type block copolymers, SCFT reveals that the synergistic effect of stretched bridging block and released packing frustration can result in the disappearance of the alternate G phase between the lamella and cylinder phases.^{45,46} The main reason is that the two effects favor the stability of the low-coordination-number (CN) cylinder phase over the alternate G phase. The two effects can also cause the absence of the G phase between the lamella and square-cylinder phases in $(BAB)_n$ star copolymers.⁴⁰ Besides the above effects resulting in the absence of the G phase, are there other effects?

In contrast to nonfrustrated ABC triblock copolymer, frustrated ABC triblock copolymer can form more complicated structures, especially hierarchical structures, thus leading to more complex self-assembly behaviors.^{47–53} “Frustrated” refers to the situation of $\chi_{AB} \sim \chi_{BC} \gg \chi_{AC}$, which favors the formation of the A/C interface of low interfacial energy to replace the portion of A/B and B/C interfaces of high interfacial energy. The presence of A/C interface is inconsistent with the A/B/C block sequence in the copolymer chain. A/C interface is generated by reducing the spread of B-subdomain sandwiched between A and C domains. In other words, B-blocks tend to form discrete domains dispersed on the A/C interface. Accordingly, the self-assembled structures consist of a main structure of A- or C-domain and substructure of B-domain. Without loss of generality, we take the A-block as minority in our discussions. For example, various hierarchical cylinder structures have been observed by experiment^{47,49,54,55} and predicted by theory,^{35,50,51} which are composed of hexagonally arranged A-cylinders decorated by different B-substructures, including spheres, double/triple helices and tripe/quadruple straight cylinders. Accordingly, the main structure should be dictated by the volume fraction of the A-block (f_A), while the substructure is controlled by the volume

fraction of the B-block (f_B). It is expected that the A-domain might follow the common transition sequence, changing from sphere to cylinder, double-gyroid, and lamella as f_A increases for a fixed low f_B . To the best of our knowledge, whether the decorating B-subdomain will change the transition sequence of A-domain has never been explored.

One interesting question is whether the decorating B-subdomain will impact the relative stability between different hierarchical structures. Since the B-subdomains are dispersed on the surface of the A-domain, the arrangement of B-subdomains should be a nontrivial factor affecting the stability of the hierarchical structures. Since the discrete B-subdomains constitute a constraint on the configurations of the ABC chain, the B-subdomains should prefer to be uniformly distributed on the surface of the A-domain to maximize the number of chain configurations. Only when the surface of the A-domain is regular and infinitely large can a uniform distribution of discrete B-subdomains be readily formed. For example, hexagonally arranged B-spheres, parallel B-cylinders, and hexagonally perforated B-lamella can be formed on the surface of A-lamella, leading to the formation of hierarchical spheres-on-lamella, cylinders-on-lamellae, and perforated lamella-on-lamella structures, respectively. In these hierarchical structures, the period of the B-substructures can be freely adjusted. However, for other surfaces whose shape has limited size in some dimensions (e.g., cylinder) or is irregular (e.g., gyroid), the arrangement of B-subdomains is frustrated or constrained. For the typical hierarchical structure consisting of A-cylinder, the B-subdomains tend to form a helical arrangement to relieve the constraint imposed by the finite circumference, which is commonly seen in the hierarchical spheres/cylinders/perforated lamella-on-cylinder structures.^{35,51} In contrast, for the rather irregular surface of the A gyroid, it is infeasible to generate a uniform arrangement of B-subdomains. Instead, there should exist different arrangements of B-subdomains, which depend on the compositional and interaction parameters. In turn, the highly frustrated arrangement of B-subdomains might lower the relative stability of the hierarchical gyroid phase over its competing cylindrical and lamellar phases, even causing it to disappear in the common transition sequence. In fact, a hierarchical gyroid structure is rarely observed in frustrated ABC triblock copolymers.

In this work, we will study the self-assembly of frustrated ABC linear triblock copolymers using the pseudospectral method of SCFT,^{56,57} focusing on the thermodynamic stability of the hierarchical gyroid phase. We will use the special initialization method to obtain the candidate phases.⁵⁸ One of the most difficult candidate phases to obtain is the hierarchical gyroid structure due to the largely variable arrangement of B-subdomains including perforated lamellae, cylinders (or helices), and spheres. We attempt to obtain different hierarchical gyroid structures using SCFT calculations with initially specialized density fields by superimposing random fluctuations onto the density fields of the core-shell gyroid morphology. Although we cannot guarantee that we find all equilibrium gyroid structures, we will find these structures that are very close to those missed equilibrium structures (i.e., with very small free energy differences) as long as we do multiple calculations. After the library of the candidate phases is constructed, it is straightforward to construct the phase diagrams with respect to the controlling parameters. The phase diagrams provide a useful guide to analyze the relative stabilities of neighboring phases.

THEORY AND METHOD

In this work, we consider an incompressible melt of ABC linear block terpolymer in a volume of V , consisting of n identical terpolymer chains. The three different blocks A, B, and C are linked by covalent bonds sequentially, with volume fractions denoted as f_A , f_B , and f_C , respectively ($f_A + f_B + f_C = 1$). The total number of segments on each terpolymer chain is specified as N , and the repulsive interactions between the three immiscible blocks are characterized by the products of N with three Flory–Huggins interaction parameters, $\chi_{AB}N$, $\chi_{BC}N$, and $\chi_{AC}N$. For simplicity, we assume that the three different blocks have an equal Kuhn length b and segment density ρ_0 . We specifically consider frustrated ABC triblock copolymers with $\chi_{AC}N < \chi_{AB}N \approx \chi_{BC}N$ and concentrate on the formation of hierarchical structures, in which each hierarchical structure is composed of main structure A-cylinder/gyroid/lamella decorated by different geometrical shapes of B-subdomains. In the standard framework of SCFT of ideal Gaussian chain model,⁵⁹ the free energy functional per chain of an ABC terpolymer melt at temperature T can be expressed as

$$\begin{aligned} \frac{F}{nk_B T} = & -\ln Q + \frac{1}{V} \int d\mathbf{r} \{ \chi_{AB} N \phi_A(\mathbf{r}) \phi_B(\mathbf{r}) \\ & + \chi_{AC} N \phi_A(\mathbf{r}) \phi_C(\mathbf{r}) + \chi_{BC} N \phi_B(\mathbf{r}) \phi_C(\mathbf{r}) \\ & - w_A(\mathbf{r}) \phi_A(\mathbf{r}) - w_B(\mathbf{r}) \phi_B(\mathbf{r}) \\ & - w_C(\mathbf{r}) \phi_C(\mathbf{r}) - \eta(\mathbf{r}) [1 - \phi_A(\mathbf{r}) - \phi_B(\mathbf{r}) \\ & - \phi_C(\mathbf{r})] \} \end{aligned} \quad (1)$$

where $V = nN/\rho_0$ and k_B is the Boltzmann constant. In the above equation, $\phi_K(\mathbf{r})$ ($K = A, B$, and C) is the spatial distribution of the volume fraction of K -block, while $w_K(\mathbf{r})$ is its conjugate potential field. $\eta(\mathbf{r})$ is a Lagrange multiplier used to enforce the incompressibility condition, $\phi_A(\mathbf{r}) + \phi_B(\mathbf{r}) + \phi_C(\mathbf{r}) = 1$. The constant quantity Q is the partition function of a single chain interacting with the mean fields of $w_A(\mathbf{r})$, $w_B(\mathbf{r})$, and $w_C(\mathbf{r})$, which can be expressed as

$$Q = \frac{1}{V} \int d\mathbf{r} q(\mathbf{r}, s) q^\dagger(\mathbf{r}, s) \quad (2)$$

Here, $q(\mathbf{r}, s)$ and $q^\dagger(\mathbf{r}, s)$ are the propagator functions of the polymer chain, indicating the probability of finding the s -segment on the chain contour at spatial position \mathbf{r} starting from the free ends of A-block and C-block, respectively. They satisfy the following modified diffusion equations

$$\frac{\partial q(\mathbf{r}, s)}{\partial s} = \nabla^2 q(\mathbf{r}, s) - w(\mathbf{r}, s) q(\mathbf{r}, s) \quad (3)$$

$$-\frac{\partial q^\dagger(\mathbf{r}, s)}{\partial s} = \nabla^2 q^\dagger(\mathbf{r}, s) - w(\mathbf{r}, s) q^\dagger(\mathbf{r}, s) \quad (4)$$

In the above equations, $w(\mathbf{r}, s) = w_K(\mathbf{r})$ when s belongs to the K -block, and the initial conditions are $q(\mathbf{r}, 0) = 1$ and $q^\dagger(\mathbf{r}, 1) = 1$.

Minimization of the free energy gives rise to standard SCFT equations as

$$w_A(\mathbf{r}) = \chi_{AB} N \phi_B(\mathbf{r}) + \chi_{AC} N \phi_C(\mathbf{r}) + \eta(\mathbf{r}) \quad (5)$$

$$w_B(\mathbf{r}) = \chi_{AB} N \phi_A(\mathbf{r}) + \chi_{BC} N \phi_C(\mathbf{r}) + \eta(\mathbf{r}) \quad (6)$$

$$w_C(\mathbf{r}) = \chi_{AC} N \phi_A(\mathbf{r}) + \chi_{BC} N \phi_B(\mathbf{r}) + \eta(\mathbf{r}) \quad (7)$$

$$\phi_A(\mathbf{r}) = \frac{1}{Q} \int_0^{f_A} ds q(\mathbf{r}, s) q^\dagger(\mathbf{r}, s) \quad (8)$$

$$\phi_B(\mathbf{r}) = \frac{1}{Q} \int_{f_A}^{f_A+f_B} ds q(\mathbf{r}, s) q^\dagger(\mathbf{r}, s) \quad (9)$$

$$\phi_C(\mathbf{r}) = \frac{1}{Q} \int_{f_A+f_B}^1 ds q(\mathbf{r}, s) q^\dagger(\mathbf{r}, s) \quad (10)$$

To analyze the relative stability between different phases, it is often to divide the free energy into different contributions, such as the entropic contribution ($-TS$) and total interaction energy (U_{tot}). For the ABC triblock copolymer systems, the free energy can be divided into the following four parts, including A/B interaction energy (U_{AB}), B/C interaction energy (U_{BC}), A/C interaction energy (U_{AC}), and entropic contribution ($-TS$).

$$\frac{U_{\text{tot}}}{nk_B T} = \frac{U_{AB} + U_{AC} + U_{BC}}{nk_B T} \quad (11)$$

$$\begin{aligned} = & \frac{1}{V} \int d\mathbf{r} \{ \chi_{AB} N \phi_A(\mathbf{r}) \phi_B(\mathbf{r}) + \chi_{AC} N \phi_A(\mathbf{r}) \phi_C(\mathbf{r}) \\ & + \chi_{BC} N \phi_B(\mathbf{r}) \phi_C(\mathbf{r}) \} \end{aligned} \quad (12)$$

$$\begin{aligned} -\frac{S}{nk_B} = & -\ln Q + \frac{1}{V} \int d\mathbf{r} \{ -w_A(\mathbf{r}) \phi_A(\mathbf{r}) - w_B(\mathbf{r}) \phi_B(\mathbf{r}) \\ & - w_C(\mathbf{r}) \phi_C(\mathbf{r}) \} \end{aligned} \quad (13)$$

$$\frac{U_{AB}}{nk_B T} = \frac{1}{V} \int d\mathbf{r} \{ \chi_{AB} N \phi_A(\mathbf{r}) \phi_B(\mathbf{r}) \} \quad (14)$$

$$\frac{U_{AC}}{nk_B T} = \frac{1}{V} \int d\mathbf{r} \{ \chi_{AC} N \phi_A(\mathbf{r}) \phi_C(\mathbf{r}) \} \quad (15)$$

$$\frac{U_{BC}}{nk_B T} = \frac{1}{V} \int d\mathbf{r} \{ \chi_{BC} N \phi_B(\mathbf{r}) \phi_C(\mathbf{r}) \} \quad (16)$$

Moreover, it is also useful to decompose the overall entropic contribution into different contributions associated with each block (A, B, and C) or each junction point (A/B and B/C), including translational entropy of A/B-junction point ($-TS_{A/B}$), translational entropy of B/C-junction point ($-TS_{B/C}$), configurational entropy of A block ($-TS_A$), configurational entropy of B block ($-TS_B$), and configurational entropy of C block ($-TS_C$), which are given by⁶⁰

$$\begin{aligned} F = & U_{\text{tot}} - TS \\ = & U_{\text{tot}} - T(S_{A/B} + S_{B/C} + S_A + S_B + S_C) \end{aligned} \quad (17)$$

$$-\frac{S_{A/B}}{nk_B} = \frac{1}{V} \int d\mathbf{r} \rho_{A/B}(\mathbf{r}) \ln \rho_{A/B}(\mathbf{r}) \quad (18)$$

$$-\frac{S_{B/C}}{nk_B} = \frac{1}{V} \int d\mathbf{r} \rho_{B/C}(\mathbf{r}) \ln \rho_{B/C}(\mathbf{r}) \quad (19)$$

$$-\frac{S_A}{nk_B} = -\frac{1}{V} \int d\mathbf{r} \{ \rho_{A/B}(\mathbf{r}) \ln q(\mathbf{r}, f_A) + w_A(\mathbf{r}) \phi_A(\mathbf{r}) \} \quad (20)$$

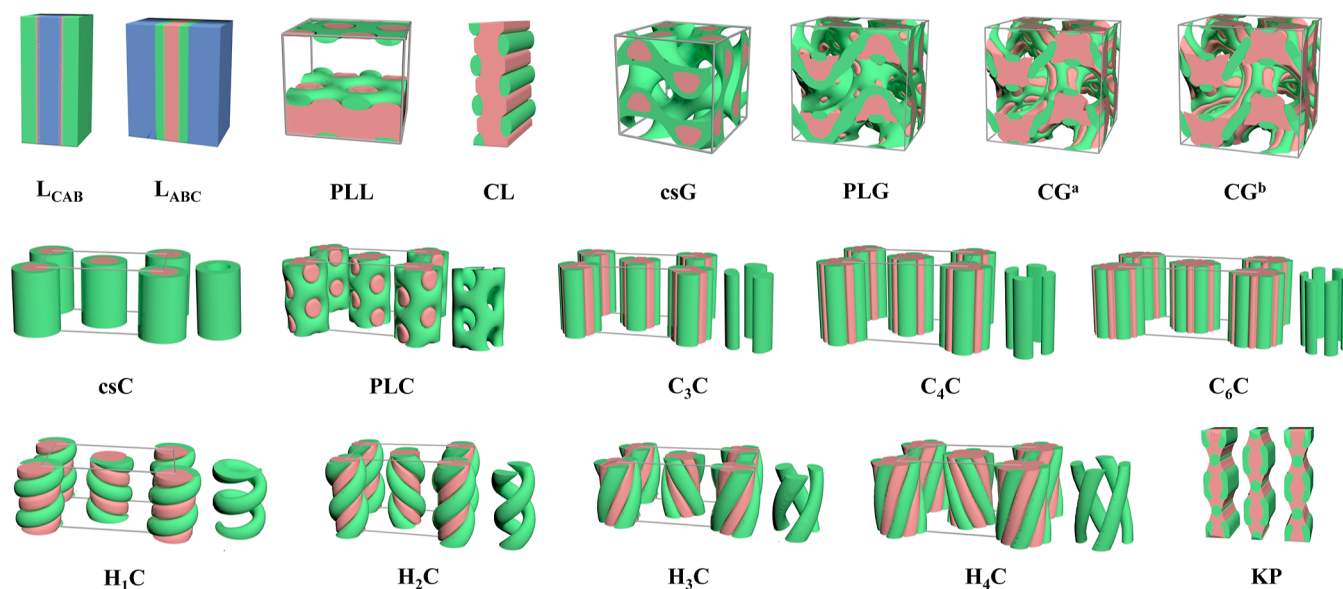


Figure 1. Considered ordered phases including ABC three-color lamella (L_{ABC}), CAB three-color lamella (L_{CAB}), perforated lamella-on-lamella (PLL), cylinders-on-lamella (CL), core-shell gyroid (csG), perforated lamella-on-gyroid (PLG), two cylinders-on-gyroid (CG^a and CG^b), core-shell cylinder (csC), perforated lamella-on-cylinder (PLC), three/four/six straight cylinders-on-cylinder ($C_3C/C_4C/C_6C$), single/double/triple/quadruple helices-on-cylinder ($H_1C/H_2C/H_3C/H_4C$), and knitting pattern (KP), in which red, green, and blue represent A, B, and C domains, respectively.

$$-\frac{S_C}{nk_B} = -\frac{1}{V} \int d\mathbf{r} \{ \rho_{B/C}(\mathbf{r}) \ln q^\dagger(\mathbf{r}, f_A + f_B) + w_C(\mathbf{r}) \phi_C(\mathbf{r}) \} \quad (21)$$

$$-\frac{S_B}{nk_B} = -\frac{1}{V} \int d\mathbf{r} \{ \rho_{B/C}(\mathbf{r}) \ln q(\mathbf{r}, f_A + f_B) + w_A(\mathbf{r}) \phi_A(\mathbf{r}) + w_B(\mathbf{r}) \phi_B(\mathbf{r}) \} - \left(-\frac{S_{A/B}}{nk_B} \right) - \left(-\frac{S_A}{nk_B} \right) \quad (22)$$

$$\rho_{A/B}(\mathbf{r}) = \frac{1}{Q} q(\mathbf{r}, f_A) q^\dagger(\mathbf{r}, f_A) \quad (23)$$

$$\rho_{B/C}(\mathbf{r}) = \frac{1}{Q} q(\mathbf{r}, f_A + f_B) q^\dagger(\mathbf{r}, f_A + f_B) \quad (24)$$

In the above expressions, $\rho_{A/B}(\mathbf{r})$ and $\rho_{B/C}(\mathbf{r})$ are the distributions of the A/B- and B/C-junction points, respectively. We choose the radius of gyration of an unperturbed polymer chain with N segments, $R_g = N^{1/2}b/\sqrt{6}$, as the unit of spatial length. In our calculations, the pseudospectral method^{56,57} is used to solve the modified diffusion equations, and the Anderson-mixing scheme is used to speed up the converging of the iteration process.^{61,62} The grid spacing is chosen to be smaller than $0.2R_g$ by using a lattice of 128×128 for the 2D phases, 96^3 for Gyroid phases, and 64^3 for the other 3D phases. We use the simple trapezoidal integration algorithm to do the integral over s in eq 8. Usually, we fix the $\Delta s = 0.01$. When the volume fraction f of one block cannot be exactly divided into an integer number of pieces, e.g., $f = 0.235$, we use 24 points to divide it. The first 23 pieces are $\Delta s = 0.01$, while the last piece is $\Delta s = 0.005$.

RESULTS AND DISCUSSION

Phase diagrams are important for understanding the self-assembly behavior of block copolymers. Assumption of the candidate phases is crucial for the construction of the phase diagram. We generate the candidate phases by assuming that both the main A-structure and B-substructure follow the common transition sequence of sphere \rightarrow cylinder \rightarrow gyroid \rightarrow lamella.^{63–66} Note that B-subdomain cannot form the three-dimensional gyroid structure and only exhibits the transition sequence of sphere \rightarrow cylinder \rightarrow perforated lamella \rightarrow lamella as its volume fraction increases due to the constraint of the surface of A-domain.⁶⁷ Moreover, it does not have the inverse transition of lamella \rightarrow perforated lamella \rightarrow cylinder \rightarrow sphere.

All of the candidate phases we assumed and generated by the special initialization scheme are listed in Figure 1. There are four lamella-type structures, including ABC three-color lamella (L_{ABC}), CAB three-color lamella (L_{CAB}), perforated lamella-on-lamella (PLL), and cylinders-on-lamella (CL). Since the spheres-on-lamella (SL) phase has a very tiny stable region in our considered system, we just ignore it. According to the similar transformation sequence of B-subdomain, we considered core-shell gyroid (csG), perforated lamella-on-gyroid (PLG), and two cylinders-on-gyroid (CG^a and CG^b) morphologies. It is necessary to stress that there may be more different PLG and CG morphologies. Through multiple searches for SCFT solutions, we find only one converged PLG phase. Though we find other CG morphologies, the CG^a or CG^b phase always has the lowest free energy among them. The most diverse class of candidate phases is cylinder-type, of which the cylinders-on-cylinder structures are very rich because the number of B-cylinders on each A-cylinder and their arrangements can be varied. We considered nine cylinder-type morphologies, including core-shell cylinder (csC), perforated lamella-on-cylinder (PLC), three/four/six straight cylinders-on-cylinder ($C_3C/C_4C/C_6C$), and single/double/

triple/quadruple helices-on-cylinder ($H_1C/H_2C/H_3C/H_4C$). An exceptional cylinder phase considered is the knitting pattern (KP), which was discovered by experiment^{68,69} and was verified by SCFT calculations⁵⁰ in frustrated ABC triblock copolymers. Since we concentrate on the stability of the hierarchical gyroid phases, we only consider their possible competing phases, the lamella- and cylinder-type phases, and do not consider the sphere-type phases.

In the previous work, Li et al. have studied the emergence and stability of various hierarchical cylinder structures in frustrated ABC linear triblock copolymers.³⁵ As they concentrated on the compositional region of hierarchical cylinders, they did not consider the hierarchical gyroid structure. To examine the formation of hierarchical gyroid structures as well as the relevant transition sequence, we expand the compositional region of the triangular phase diagram; that is, the volume fractions of main A-domain and B-subdomain range from 0.17 to 0.35 ($0.17 \leq f_A \leq 0.35$) and from 0.12 to 0.35 ($0.12 \leq f_B \leq 0.35$), respectively. Notably, in such a wide range of volume fraction, B-subdomain experiences the transition from cylinder to perforated lamella and lamella, enabling one to study the impact of different B-subdomains on the stability of hierarchical structures.

The triangular phase diagram for $\chi_{AB}N = \chi_{BC}N = 80$ and $\chi_{AC}N = 15$ constructed by SCFT calculations to include all the candidate phases in Figure 1 is shown in Figure 2. This phase

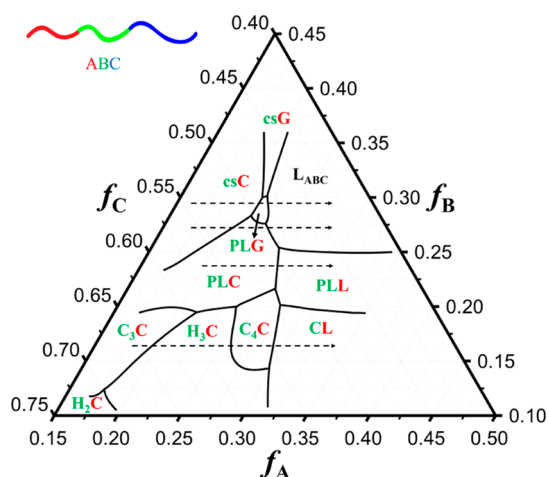


Figure 2. Part of the triangular phase diagram of the frustrated ABC linear triblock copolymer with $\chi_{AB}N = \chi_{BC}N = 80$ and $\chi_{AC}N = 15$, mainly composed of A-domains decorated by different B-substructures.

diagram consists of 11 stable morphologies, including csC, csG, L_{ABC} , PLG, PLC, PLL, C_3C , H_3C , H_2C , C_4C , and CL. One of the most remarkable features is that only one hierarchical gyroid structure, i.e., perforated gyroid (PLG), appears and its phase region located between the csC and L_{ABC} phases is narrow. Specifically, these hierarchical cylindrical phases, such as PLC, C_4C , and H_3C , directly transfer to the corresponding hierarchical lamellar phases (PLL and CL) without going through any hierarchical gyroid phase. This observation indicates that the transitions of these hierarchical phases do not simply follow the common transition sequence of cylinder \rightarrow gyroid \rightarrow lamella. In other words, the decoration of B-subdomains on the A-domains imposes a nontrivial effect on the transition of A-domains.

Besides the absence of the hierarchical gyroid structure in a large region, the phase diagram consists of many other interesting transitions. The top area of the phase diagram shows a transition sequence of csC \rightarrow csG \rightarrow L_{ABC} . In this area, the B-block with $f_B \gtrsim 0.3$ forms a complete layer covering the A-domains, leading to the formation of core-shell structures in the C-matrix. The addition of the B-shell onto the A-core does not change the symmetry of these structures and thus does not affect the common transition sequence. As f_B decreases, the complete layer tends to be perforated. In the range of $0.28 < f_B < 0.30$, the csC morphology with the increase in f_A transfers to PLG and then to L_{ABC} . Surprisingly, the transition of B-subdomains along this transition sequence is nonunidirectional, transforming from a complete layer to perforated layer and back to a complete layer for fixed f_B . The similar nonunidirectional transition of B-subdomains is also observed in the transition from csC to PLC and to L_{ABC} in the range of $0.25 < f_B < 0.28$. This observation suggests that the change in f_A simultaneously causes the transition of B-subdomains.

The transition of B-subdomains from the complete layer to the perforated layer and even to discrete domains can be seen as a “wettability” phenomenon, changing from wetting to dewetting gradually. The nonunidirectional transition of B-subdomains should result from two different factors. From the csC \rightarrow PLC transition, we can speculate that the key factor causing the transformation of the B-subdomain is the curvature of A-domain. For a given f_B , the smaller the curvature of the A-domain, the thinner the B-subdomain covering it, and the easier the B-subdomain is to be perforated like “dewetting”. The transition from PLG or PLC to L_{ABC} implies that the abrupt transformation of the A-domain is another important factor impacting the formation of B-subdomains. Since the formation of holes within the B-subdomain is to lower the interaction energy by replacing the A/B and B/C interfaces of high interfacial tension with the A/C interface of low interfacial tension, the necessity to form a perforated layer decreases accordingly as the overall interaction energy decreases along the transition from PLG or PLC to L_{ABC} .

Though the compositional effect on the interfacial curvature of the B-block in ABC triblock is not as clear as that in the AB diblock due to its connection to both A and C blocks, the B-block should tend to form the B-subdomain with the A/B and B/C interfaces of increasing curvature as f_B decreases. This is why in the phase diagram, from top to bottom, the B-subdomain changes from layer to perforated layer and then to straight/helical cylinders. The “wettability” analogy may provide a more intuitive scenario for the transition of B-subdomains induced by the change of f_B .⁷⁰ Nevertheless, the transition from wetting to dewetting is driven by the enthalpy contribution, disfavoring the chain configurations. For a longer B-block, the dewetting is associated with more severe entropy loss and thus is less likely to occur.

In the range of $0.2 \lesssim f_B \lesssim 0.25$, the PLC morphology transfers to the PLL morphology with increasing f_A , along which the A-domain changes from cylinder to lamella, while the B-subdomain remains the PL structure. When f_B is reduced to $0.15 \lesssim f_B \lesssim 0.2$, the B-block prefers to form cylinders, leading to the transition sequence of $C_3C \rightarrow H_3C \rightarrow C_4C \rightarrow CL$ along increasing f_A . As f_B decreases further, the region of C_4C disappears, giving rise to the direct transition from H_3C to CL. Previous work has elucidated that the relative stability between these different cylinders-on-cylinder morphologies

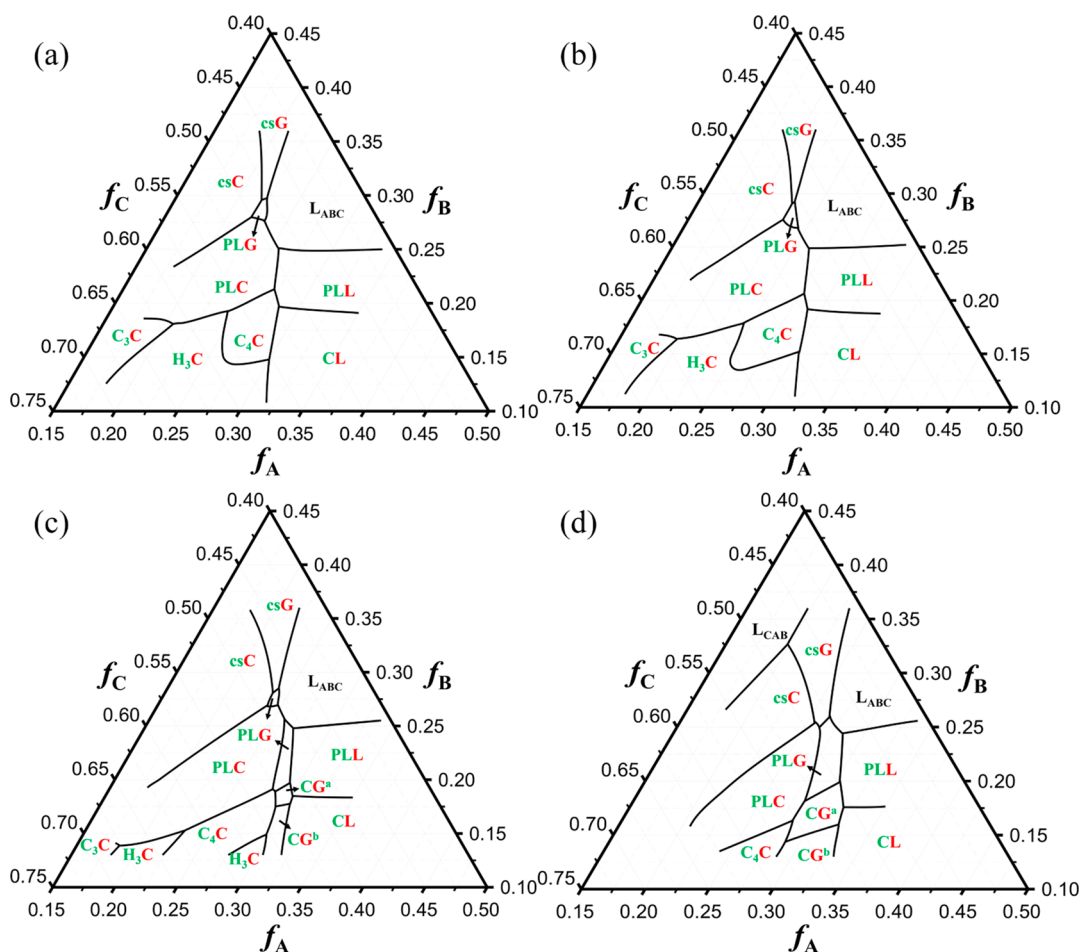


Figure 3. Triangular phase diagrams of the frustrated ABC linear triblock copolymer for $\chi_{AB}N = 70$ (a), 60 (b), 50 (c), and 40 (d) with fixed $\chi_{BC}N = 80$ and $\chi_{AC}N = 15$.

(C_3C , C_4C , H_2C , and H_3C) is mainly controlled by the length ratio of the B-cylinder to the core A-cylinder.³⁵ Therefore, one of the unusual phase transition features most urgently in need of explanation in this phase diagram is the absence of the hierarchical gyroid phase for $f_B < 0.28$.

In order to understand the absence of the hierarchical gyroid structure, we vary the interaction parameter $\chi_{AB}N$ to see whether the gyroid morphology can appear. We can infer that as $\chi_{AB}N$ decreases, the self-assembly behavior of ABC triblock copolymer would gradually approach the AB diblock. In other words, the gyroid structure is more likely to form. Accordingly, we have constructed the triangular phase diagrams for various values of $\chi_{AB}N = 70, 60, 50,$ and 40 shown in Figure 3, while keeping the other parameters the same as in Figure 2. Comparing the four phase diagrams, we find that the transition boundaries with respect to f_B shift down to small f_B as $\chi_{AB}N$ decreases. This is because the tendency to form A/C interface in replacement of the A/B and B/C interfaces declines as the A/B interaction energy decreases. Until $\chi_{AB}N$ is lowered to 50, the hierarchical gyroid structures appear between the hierarchical cylindrical and lamellar structures, leaving a narrow window of f_B in which the gyroid structure is missing. For $\chi_{AB}N = 40$, the stable region of the gyroid phases goes through the entire range of f_B . Moreover, the gyroid regions with respect to f_A expand when $\chi_{AB}N = 50$ is reduced to 40 (Figure 4).

In the two phase diagrams of $\chi_{AB}N = 50$ and 40, we observed that the B-subdomain of the gyroid structure transforms from a perforated layer to a cylinder with reducing f_B , leading to the transition of $PLG \rightarrow CG$. Note that two nearly degenerate CG morphologies are observed in our SCFT calculations.

To deeply understand the change of the relative stability of the hierarchical gyroid phase over its competing phases, we analyze the transition from C_4C to CG^a along decreasing $\chi_{AB}N$ for $f_A = 0.29$, $f_B = 0.18$, $\chi_{BC}N = 80$, and $\chi_{AC}N = 15$. We first compare the free energy (F), entropic contribution ($-TS$), total interaction energy (U_{tot}), A/B interaction energy (U_{AB}), B/C interaction energy (U_{BC}), and A/C interaction energy (U_{AC}) between the two phases. The results show that the CG^a phase has a higher entropic contribution but lower interaction energy than C_4C in the considered range of $\chi_{AB}N$, implying that the gyroid structure may be destabilized by the constraint of the nonuniformly arranged B-subdomains on the chain configurations. The continuous decrease of the difference of $-TS$ and increasing of the difference of U_{tot} confirm that the relative stability of the gyroid structure is improved by the relieved constraint on the chain configurations as $\chi_{AB}N$ decreases.

To reveal which part of the configuration of the triblock chain is mostly affected by the change of $\chi_{AB}N$, we decompose the overall entropic contribution into different parts associated with A-block, B-block, C-block, A/B-junction point, and B/C-junction point in Figure 5. Similarly, we compare these

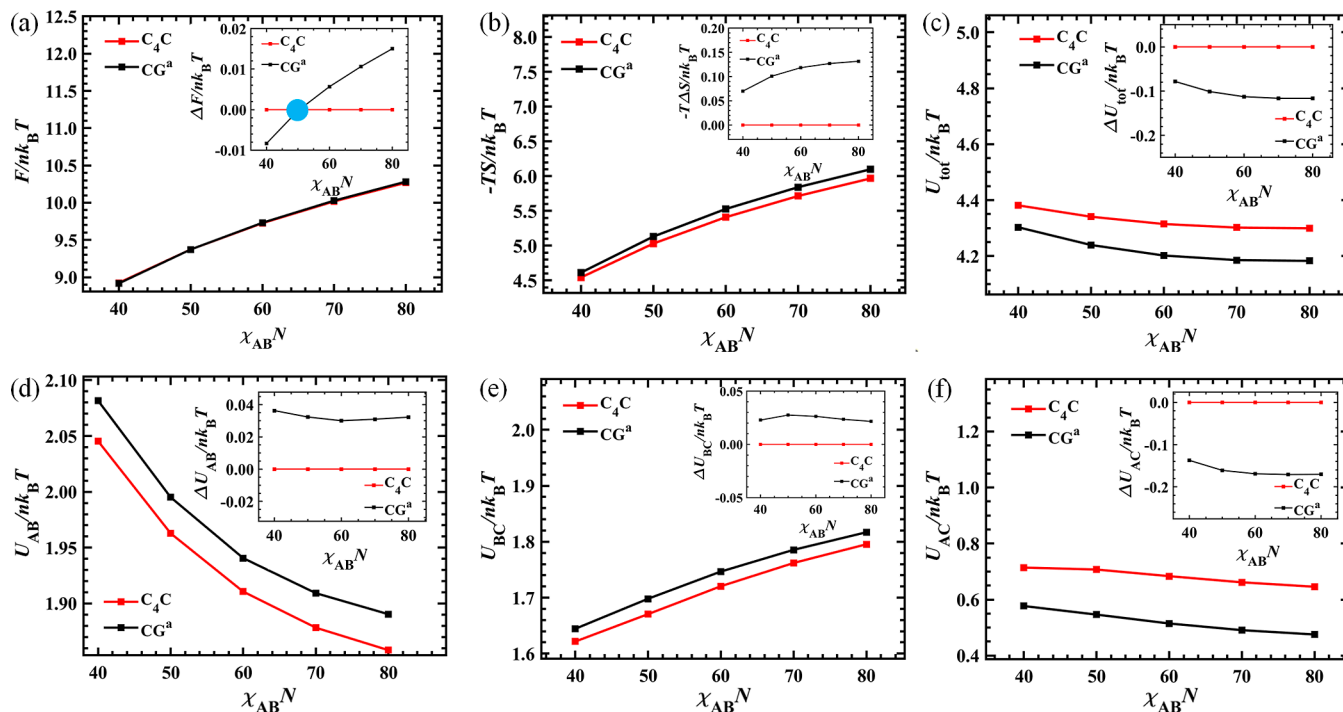


Figure 4. Comparisons of free energy as well as its different contributions between the C_4C and CG^a phases along the path of $f_A = 0.29$, $f_B = 0.18$, $\chi_{BC}N = 80$, and $\chi_{AC}N = 15$: (a) free energy (F), (b) entropic contribution ($-TS$), (c) total interaction energy (U_{tot}), (d) A/B interaction energy (U_{AB}), (e) B/C interaction energy (U_{BC}), and (f) A/C interaction energy (U_{AC}), where each inset shows the difference of the corresponding quantity.

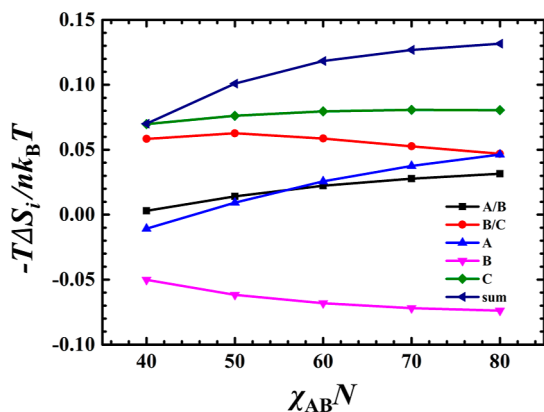


Figure 5. Comparisons of the different entropic contributions between the C_4C and CG^a phases along the path of $f_A = 0.29$, $f_B = 0.18$, $\chi_{BC}N = 80$, and $\chi_{AC}N = 15$: translational entropy of A/B-junction point ($-T\Delta S_{A/B}$), translational entropy of B/C-junction point ($-T\Delta S_{B/C}$), configurational entropy of A block ($-T\Delta S_A$), configurational entropy of B block ($-T\Delta S_B$), and configurational entropy of C block ($-T\Delta S_C$).

different entropic contributions between the CG^a and C_4C phases. Remarkably, the relative value of the entropic contribution of the A-block drops down in a trend similar to that of the overall entropic contribution as $\chi_{AB}N$ decreases. The relative magnitude of the entropic contribution of A/B-junction point also shows a similar but milder decreasing trend, while that of B-block shows an opposite variation trend and that of C-block does not change noticeably. These results evidence that the configuration of the A-block is mostly affected by $\chi_{AB}N$. When $\chi_{AB}N$ is reduced, the A/B interface becomes more diffuse, or the A/B-junction point can access

more space. As a consequence, the A-block can access more possible configurations, especially it can extend to fill the far space at the center of the node of the gyroid structure without causing extra stretching.

To understand the change in the interaction energy common to different morphologies, we take the C_4C structure as an example to illustrate the density distributions as well as the spatial distributions of the A/B-junction points and B/C-junction points for $\chi_{AB}N = 80, 60$, and 40 in Figure 6. As $\chi_{AB}N$ decreases, the C_4C structure exhibits two remarkable features. One feature is that the A/B interface becomes wide and diffuse due to the reduced segregation strength between the A and B blocks. The other is that the B-subdomain moves gradually from the A/C interface into the A-domain, lowering the B/C interaction energy at the cost of the A/B interaction energy. This is why the A/B interaction energy ascends as $\chi_{AB}N$ decreases. It is necessary to mention that the B/C interface also becomes more diffuse as $\chi_{AB}N$ decreases though $\chi_{BC}N$ is fixed. This is because more and more A-blocks enter the interstitial space between the B- and C-domains as the B-domain moves into the A-domain.

Apparently, with the decrease in $\chi_{AB}N$, the distributions of A/B-junction points in the middle row of the panels from right to left in Figure 6 become less concentrated, indicating that some portion of A/B-junction points is withdrawn into A-domain. As a consequence, the A/B interfaces in the top row of the panels from right to left become more and more diffuse. In contrast, the distributions of the B/C-junction points do not change notably with $\chi_{AB}N$ due to the unchanged $\chi_{BC}N$. Moreover, the density distributions in the top row of Figure 6 suggest that the B-subdomains gradually move into the A-domain as $\chi_{AB}N$ decreases. At low $\chi_{AB}N = 40$, the B-

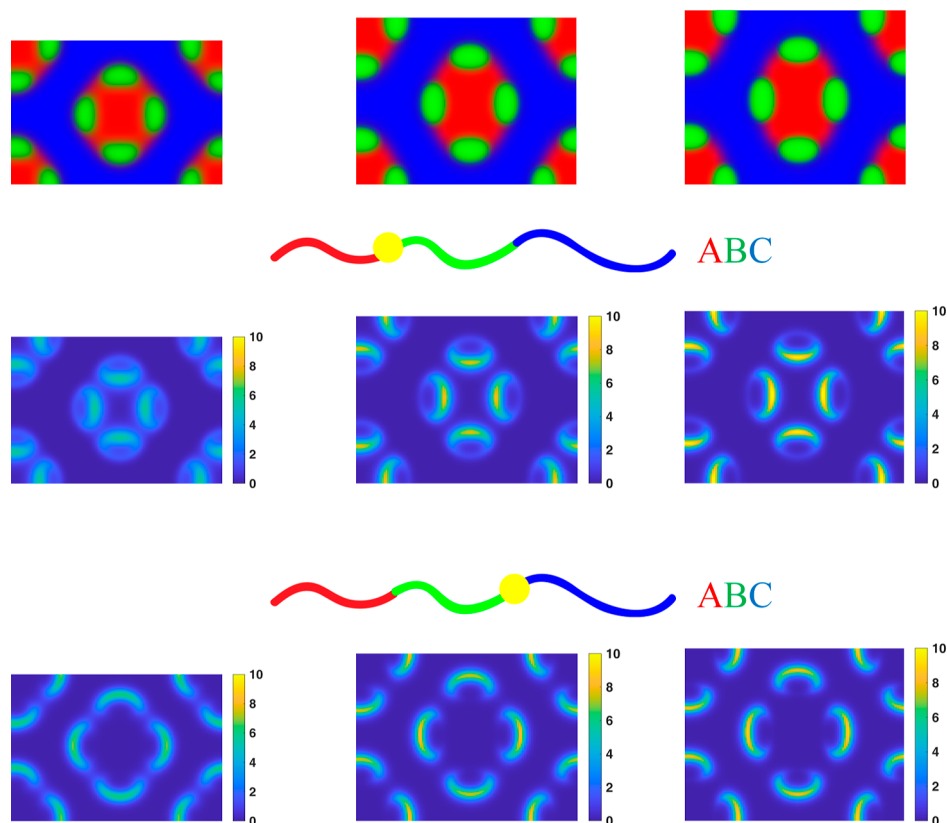


Figure 6. Density distributions plots (top row), spatial distributions of the A/B-junction points (middle row), and B/C-junction points (bottom row) for ABC linear triblock copolymer at fixed $f_A = 0.29$, $f_B = 0.18$, $\chi_{BC}N = 80$, and $\chi_{AC}N = 15$ in the C_4C morphology for $\chi_{AB}N = 40$ (left column), 60 (central column), and 80 (right column).

subdomains are nearly embedded in the A-domain, increasing A/B and A/C interfaces but adding chain configurations.

Based on these results, we can draw schematics in Figure 7 to illustrate the change of the chain configurations with

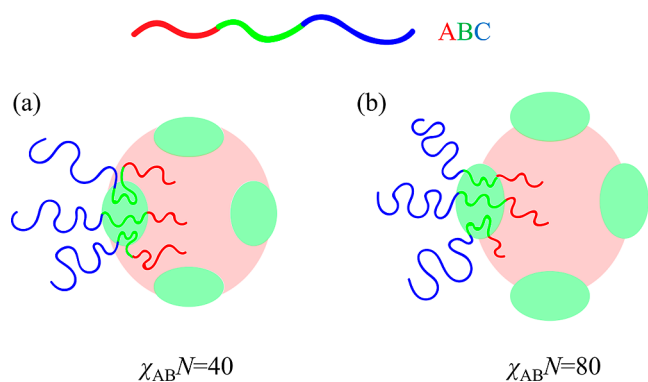


Figure 7. Schematics illustrating the change of the chain configurations of ABC triblock copolymer with changing $\chi_{AB}N$ in the four cylinders-on-cylinder morphology.

reducing $\chi_{AB}N$. At high $\chi_{AB}N = 80$, A/B-junction points are highly concentrated to form sharp A/B interfaces (right panel), while at weak $\chi_{AB}N = 40$, some A/B-junction points enter the A-domain to add the chain configurations at the low cost of A/B interaction energy. In other words, the diffused distribution of A/B-junction points relieves the constraint of B-subdomains on the chain configurations, thus improving the stability of the hierarchical gyroid phases relative to their competing phases.

In particular, the entrance of some A/B-junction points is favorable to release the high stretching of A-blocks that fill the central area of the large node of the gyroid structure. As long as the gain in the entropic contribution from the released constraint on the chain configurations can compensate the penalty of A/B and A/C interaction energy by lowering $\chi_{AB}N$, the hierarchical gyroid structure becomes stable in the phase region between the hierarchical cylindrical and lamellar structures.

To further demonstrate the effect of $\chi_{AB}N$ on the stability of the hierarchical gyroid structures, we construct the phase diagram with respect to f_A and $\chi_{AB}N$ for fixed $f_B = 0.18$, $\chi_{BC}N = 80$ and $\chi_{AC}N = 15$. In Figure 8, the transitions with the decrease in $\chi_{AB}N$ are mainly induced by the transformation of the B-subdomain within the phase diagram regions where $f_A \lesssim$

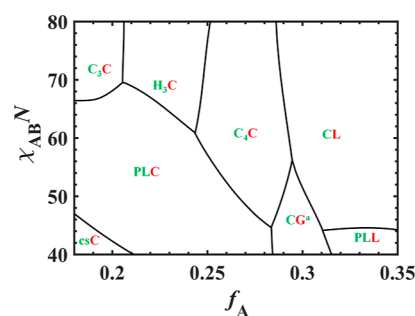


Figure 8. Phase diagram in the $\chi_{AB}N - f_A$ plane for the ABC linear triblock copolymer with $\chi_{AB}N$ decreasing from 80 to 40 for fixed $f_B = 0.18$, $\chi_{BC}N = 80$, and $\chi_{AC}N = 15$.

0.285 and $f_A \gtrsim 0.315$. That is, C₃C/H₃C/C₄C transfer to PLC and then to csC in the left part of $f_A \lesssim 0.285$, and CL transfers to PLL in the region of $f_A \gtrsim 0.315$. In contrast, along the transitions from C₄C/CL to CG^a occurred in the middle part of $0.285 < f_A < 0.315$, the A-domain changes from cylinder/lamella to gyroid, while the B-subdomain is unchanged. This observation confirms that the hierarchical gyroid structure appears between the hierarchical cylindrical and lamellar structures with respect to f_A only when the constraint of the discrete B-subdomains on the chain configurations is relieved by lowering $\chi_{AB}N$.

CONCLUSIONS

In summary, we have investigated the self-assembly of frustrated ABC triblock copolymers using SCFT, focusing on the stability of hierarchical gyroid structures. Since these hierarchical gyroid nanostructures may be used to fabricate functional materials with high performance, it is critical to choose the A, B, and C monomers for obtaining three proper Flory–Huggins parameters based on the phase diagram. Specifically, we consider that short middle B-blocks form discrete subdomains decorated on the surface of A-domain. We first construct the corresponding part of the triangular phase diagram with respect to three compositions (f_A , f_B , and f_C) for fixed $\chi_{AB}N = \chi_{BC}N = 80 > \chi_{AC}N = 15$. The phase transitions in the phase diagram can be induced by the transformation of either the B-subdomain or A-domain. Surprisingly, the hierarchical gyroid structure is not commonly formed between the hierarchical cylindrical and lamellar structures in the transition sequence with changing f_A . For these hierarchical structures, the formation of B-subdomains on the surfaces of A-domains presents a constraint on the chain configurations, leading to entropy loss. Accordingly, we speculate that the absence of the gyroid structure is mainly caused by its irregular surface of the A-domain that does not allow the B-subdomain to form a uniform arrangement and thus produces more severe constraint on the chain configurations than the cylindrical and lamellar structures with regular surfaces of A-domains.

In order to further understand the stability of the hierarchical gyroid structure, we reduce $\chi_{AB}N$ to 70, 60, 50, and 40, and construct the corresponding phase diagrams. At $\chi_{AB}N = 50$, the hierarchical gyroid structure starts to form between the hierarchical cylindrical and lamellar structures along increasing f_A , giving rise to the common transformation from cylinder to gyroid and then to lamella for A-domain. When $\chi_{AB}N$ decreases to 40, the stable window of the gyroid structures widens. By comparing the different parts of the free energy as well as the different parts of the entropic contribution associated with each block and each junction point, we find that the change of the relative stability of the gyroid structure is mainly contributed by the entropic contribution, especially the part contributed by the A-block. This work demonstrates that the transition sequence from the cylinder to the gyroid and lamella, which is commonly observed in many simple block copolymers, may be disrupted by the formation of substructures for hierarchical structures.

AUTHOR INFORMATION

Corresponding Authors

Qingshu Dong – State Key Laboratory of Molecular Engineering of Polymers, Key Laboratory of Computational Physical Sciences, Department of Macromolecular Science,

Fudan University, Shanghai 200433, China;

Email: qsdong@fudan.edu.cn

Weihua Li – State Key Laboratory of Molecular Engineering of Polymers, Key Laboratory of Computational Physical Sciences, Department of Macromolecular Science, Fudan University, Shanghai 200433, China; orcid.org/0000-0002-5133-0267; Email: weihuali@fudan.edu.cn

Authors

Xintong You – State Key Laboratory of Molecular Engineering of Polymers, Key Laboratory of Computational Physical Sciences, Department of Macromolecular Science, Fudan University, Shanghai 200433, China

Meijiao Liu – Key Laboratory of Surface & Interface Science of Polymer Materials of Zhejiang Province, School of Chemistry and Chemical Engineering, Zhejiang Sci-Tech University, Hangzhou, Zhejiang 310018, China; orcid.org/0000-0001-5056-2915

Complete contact information is available at:

<https://pubs.acs.org/10.1021/acs.macromol.3c01247>

Notes

The authors declare no competing financial interest.

ACKNOWLEDGMENTS

This work was supported by the National Natural Science Foundation of China (grant nos. 21925301 and 22203018).

REFERENCES

- (1) Bates, F. S.; Fredrickson, G. H. Block Copolymers-Designer Soft Materials. *Phys. Today* **1999**, *52*, 32–38.
- (2) Simon, P. F. W.; Ulrich, R.; Spiess, H. W.; Wiesner, U. Block Copolymer-Ceramic Hybrid Materials from Organically Modified Ceramic Precursors. *Chem. Mater.* **2001**, *13*, 3464–3486.
- (3) Bates, F. S.; Hillmyer, M. A.; Lodge, T. P.; Bates, C. M.; Delaney, K. T.; Fredrickson, G. H. Multiblock Polymers: Panacea or Pandora's Box? *Science* **2012**, *336*, 434–440.
- (4) Bates, C. M.; Bates, F. S. 50th Anniversary Perspective: Block Polymers-Pure Potential. *Macromolecules* **2017**, *50*, 3–22.
- (5) Polymeropoulos, G.; Zapsas, G.; Ntetsikas, K.; Bilalis, P.; Gnanou, Y.; Hadjichristidis, N. 50th Anniversary Perspective: Polymers with Complex Architectures. *Macromolecules* **2017**, *50*, 1253–1290.
- (6) Lu, Y. Q.; Lin, J. P.; Wang, L. Q.; Zhang, L. S.; Cai, C. H. Self-Assembly of Copolymer Micelles: Higher-Level Assembly for Constructing Hierarchical Structure. *Chem. Rev.* **2020**, *120*, 4111–4140.
- (7) Müller, M.; Abetz, V. Nonequilibrium Processes in Polymer Membrane Formation: Theory and Experiment. *Chem. Rev.* **2021**, *121*, 14189–14231.
- (8) Huang, C. H.; Zhu, Y. Y.; Man, X. K. Block Copolymer Thin Films. *Phys. Rep.* **2021**, *932*, 1–36.
- (9) Matsen, M. W. The Standard Gaussian Model for Block Copolymer Melts. *J. Phys.: Condens. Matter* **2002**, *14*, R21–R47.
- (10) Matsen, M. W.; Schick, M. Microphases of a Diblock Copolymer with Conformational Asymmetry. *Macromolecules* **1994**, *27*, 4014–4015.
- (11) Matsen, M. W.; Bates, F. S. Unifying Weak- and Strong-Segregation Block Copolymer Theories. *Macromolecules* **1996**, *29*, 1091–1098.
- (12) Tyler, C. A.; Morse, D. C. Orthorhombic Fddd Network in Triblock and Diblock Copolymer Melts. *Phys. Rev. Lett.* **2005**, *94*, 208302.
- (13) Cochran, E. W.; Garcia-Cervera, C. J.; Fredrickson, G. H. Stability of the Gyroid Phase in Diblock Copolymers at Strong Segregation. *Macromolecules* **2006**, *39*, 2449–2451.

- (14) Hajduk, D. A.; Harper, P. E.; Gruner, S. M.; Honeker, C. C.; Kim, G.; Thomas, E. L.; Fetters, L. J. The Gyroid-A New Equilibrium Morphology in Weakly Segregated Diblock Copolymers. *Macromolecules* **1994**, *27*, 4063–4075.
- (15) Maldovan, M.; Urbas, A. M.; Yufa, N.; Carter, W. C.; Thomas, E. L. Photonic Properties of Bicontinuous Cubic Microphases. *Phys. Rev. B: Condens. Matter Mater. Phys.* **2002**, *65*, 165123.
- (16) Werner, J. G.; Hoheisel, T. N.; Wiesner, U. Synthesis and Characterization of Gyroidal Mesoporous Carbons and Carbon Monoliths with Tunable Ultralarge Pore Size. *ACS Nano* **2014**, *8*, 731–743.
- (17) Wang, H. F.; Yu, L. H.; Wang, X. B.; Ho, R. M. A Facile Method to Fabricate Double Gyroid as a Polymer Template for Nanohybrids. *Macromolecules* **2014**, *47*, 7993–8001.
- (18) Lequieu, J.; Quah, T.; Delaney, K. T.; Fredrickson, G. H. Complete Photonic Band Gaps with Nonfrustrated ABC Bottlebrush Block Polymers. *ACS Macro Lett.* **2020**, *9*, 1074–1080.
- (19) Yu, B. H.; Li, R. P.; Segalman, R. A. Tuning the Double Gyroid Phase Window in Block Copolymers Via Polymer Chain Conformation near the Interface. *Macromolecules* **2021**, *54*, 5388–5396.
- (20) Wen, T.; Yuan, J.; Lai, W.; Liu, X.; Liu, Y. L.; Chen, L. Y.; Jiang, X. Morphology-Controlled Mesopores with Hydrophilic Pore Walls from Triblock Copolymers. *Macromolecules* **2022**, *55*, 4812–4820.
- (21) Matsen, M. W. Effect of Architecture on the Phase Behavior of AB-Type Block Copolymer Melts. *Macromolecules* **2012**, *45*, 2161–2165.
- (22) Nakazawa, H.; Ohta, T. Microphase Separation of ABC-Type Triblock Copolymers. *Macromolecules* **1993**, *26*, 5503–5511.
- (23) Mogi, Y.; Nomura, M.; Kotsuji, H.; Ohnishi, K.; Matsushita, Y.; Noda, I. Superlattice Structures in Morphologies of the ABC Triblock Copolymers. *Macromolecules* **1994**, *27*, 6755–6760.
- (24) Zheng, W.; Wang, Z. G. Morphology of ABC Triblock Copolymers. *Macromolecules* **1995**, *28*, 7215–7223.
- (25) Matsen, M. W. Gyroid Versus Double-Diamond in ABC Triblock Copolymer Melts. *J. Chem. Phys.* **1998**, *108*, 785–796.
- (26) Goldacker, T.; Abetz, V. Core-Shell Cylinders and Core-Shell Gyroid Morphologies Via Blending of Lamellar ABC Triblock and BC Diblock Copolymers. *Macromolecules* **1999**, *32*, 5165–5167.
- (27) Sheffeltine, T. A.; Vigild, M. E.; Matsen, M. W.; Hajduk, D. A.; Hillmyer, M. A.; Cussler, E. L.; Bates, F. S. Core-Shell Gyroid Morphology in a Poly(isoprene-*block*-styrene-*block*-dimethylsiloxane) Triblock Copolymer. *J. Am. Chem. Soc.* **1999**, *121*, 8457–8465.
- (28) Hückstädt, H.; Göpfert, A.; Abetz, V. Influence of the Block Sequence on the Morphological Behavior of ABC Triblock Copolymers. *Polymer* **2000**, *41*, 9089–9094.
- (29) Epps, T. H.; Cochran, E. W.; Bailey, T. S.; Waletzko, R. S.; Hardy, C. M.; Bates, F. S. Ordered Network Phases in Linear Poly(isoprene-*b*-styrene-*b*-ethylene oxide) Triblock Copolymers. *Macromolecules* **2004**, *37*, 8325–8341.
- (30) Tang, P.; Qiu, F.; Zhang, H. D.; Yang, Y. L. Morphology and Phase Diagram of Complex Block Copolymers: ABC Linear Triblock Copolymers. *Phys. Rev. E: Stat., Nonlinear, Soft Matter Phys.* **2004**, *69*, 031803.
- (31) Chatterjee, J.; Jain, S.; Bates, F. S. Comprehensive Phase Behavior of Poly(isoprene-*b*-styrene-*b*-ethylene oxide) Triblock Copolymers. *Macromolecules* **2007**, *40*, 2882–2896.
- (32) Tyler, C. A.; Qin, J.; Bates, F. S.; Morse, D. C. SCFT Study of Nonfrustrated ABC Triblock Copolymer Melts. *Macromolecules* **2007**, *40*, 4654–4668.
- (33) Qin, J.; Bates, F. S.; Morse, D. C. Phase Behavior of Nonfrustrated ABC Triblock Copolymers: Weak and Intermediate Segregation. *Macromolecules* **2010**, *43*, 5128–5136.
- (34) Wang, C.; Lee, D. H.; Hexemer, A.; Kim, M. I.; Zhao, W.; Hasegawa, H.; Ade, H.; Russell, T. P. Defining the Nanostructured Morphology of Triblock Copolymers Using Resonant Soft X-Ray Scattering. *Nano Lett.* **2011**, *11*, 3906–3911.
- (35) Li, W. H.; Qiu, F.; Shi, A. C. Emergence and Stability of Helical Superstructures in ABC Triblock Copolymers. *Macromolecules* **2012**, *45*, 503–509.
- (36) Boschetti-De-Fierro, A.; Müller, A. J.; Abetz, V. Synthesis and Characterization of Novel Linear PB-*b*-PS-*b*-PEO and PE-*b*-PS-*b*-PEO Triblock Terpolymers. *Macromolecules* **2007**, *40*, 1290–1298.
- (37) Chang, A. B.; Bates, F. S. The ABCs of Block Polymers. *Macromolecules* **2020**, *53*, 2765–2768.
- (38) Dong, Q. S.; Li, W. H. Effect of Molecular Asymmetry on the Formation of Asymmetric Nanostructures in ABC-Type Block Copolymers. *Macromolecules* **2021**, *54*, 203–213.
- (39) Bates, F. S. Network Phases in Block Copolymer Melts. *MRS Bull.* **2005**, *30*, 525–532.
- (40) Chen, L.; Qiang, Y. C.; Li, W. H. Tuning Arm Architecture Leads to Unusual Phase Behaviors in a (BAB)₃ Star Copolymer Melt. *Macromolecules* **2018**, *51*, 9890–9900.
- (41) Li, C. C.; Dong, Q. S.; Li, W. H. Largely Tunable Asymmetry of Phase Diagrams of A(AB)_n Miktoarm Star Copolymer. *Macromolecules* **2020**, *53*, 10907–10917.
- (42) Grason, G. M.; Kamien, R. D. Interfaces in Diblocks: A Study of Miktoarm Star Copolymers. *Macromolecules* **2004**, *37*, 7371–7380.
- (43) Bates, M. W.; Barbon, S. M.; Levi, A. E.; Lewis, R. M.; Beech, H. K.; Vonk, K. M.; Zhang, C.; Fredrickson, G. H.; Hawker, C. J.; Bates, C. M. Synthesis and Self-Assembly of AB_n Miktoarm Star Polymers. *ACS Macro Lett.* **2020**, *9*, 396–403.
- (44) Qiang, Y. C.; Li, W. H.; Shi, A. C. Stabilizing Phases of Block Copolymers with Gigantic Spheres Via Designed Chain Architectures. *ACS Macro Lett.* **2020**, *9*, 668–673.
- (45) Li, L. Y.; Li, W. H. Effect of Branching Architecture on the Self-Assembly of Symmetric ABC-Type Block Terpolymers. *Giant* **2021**, *7*, 100065.
- (46) Li, L. Y.; Xu, Z. W.; Li, W. H. Emergence of Connected Binary Spherical Structures from the Self-Assembly of an AB₂C Four-Arm Star Terpolymer. *Macromolecules* **2022**, *55*, 9890–9899.
- (47) Krappe, U.; Stadler, R.; Voigtmartin, I. Chiral Assembly in Amorphous ABC Triblock Copolymers-Formation of a Helical Morphology in Polystyrene-*block*-polybutadiene-*block*-poly(methyl methacrylate) Block Copolymers. *Macromolecules* **1995**, *28*, 4558–4561.
- (48) Breiner, U.; Krappe, U.; Abetz, V.; Stadler, R. Cylindrical Morphologies in Asymmetric ABC Triblock Copolymers. *Macromol. Chem. Phys.* **1997**, *198*, 1051–1083.
- (49) Jinnai, H.; Kaneko, T.; Matsunaga, K.; Abetz, C.; Abetz, V. A Double Helical Structure Formed from an Amorphous, Achiral ABC Triblock Terpolymer. *Soft Matter* **2009**, *5*, 2042–2046.
- (50) Liu, M. J.; Li, W. H.; Qiu, F.; Shi, A. C. Theoretical Study of Phase Behavior of Frustrated ABC Linear Triblock Copolymers. *Macromolecules* **2012**, *45*, 9522–9530.
- (51) Zhang, Q.; Qiang, Y. C.; Duan, C.; Li, W. H. Single Helix Self-Assembled by Frustrated ABC₂ Branched Terpolymers. *Macromolecules* **2019**, *52*, 2748–2758.
- (52) Shi, A. C. Frustration in Block Copolymer Assemblies. *J. Phys.: Condens. Matter* **2021**, *33*, 253001.
- (53) Xu, Z. W.; Li, W. H. Control the Self-Assembly of Block Copolymers by Tailoring the Packing Frustration. *Chin. J. Chem.* **2022**, *40*, 1083–1090.
- (54) Higuchi, T.; Sugimori, H.; Jiang, X.; Hong, S.; Matsunaga, K.; Kaneko, T.; Abetz, V.; Takahara, A.; Jinnai, H. Morphological Control of Helical Structures of an ABC-Type Triblock Terpolymer by Distribution Control of a Blending Homopolymer in a Block Copolymer Microdomain. *Macromolecules* **2013**, *46*, 6991–6997.
- (55) Ishige, R.; Higuchi, T.; Jiang, X.; Mita, K.; Ogawa, H.; Yokoyama, H.; Takahara, A.; Jinnai, H. Structural Analysis of Microphase Separated Interface in an ABC-Type Triblock Terpolymer by Combining Methods of Synchrotron-Radiation Grazing Incidence Small-Angle X-Ray Scattering and Electron Microtomography. *Macromolecules* **2015**, *48*, 2697–2705.
- (56) Tzeremes, G.; Rasmussen, K. O.; Lookman, T.; Saxena, A. Efficient Computation of the Structural Phase Behavior of Block Copolymers. *Phys. Rev. E: Stat. Phys., Plasmas, Fluids, Relat. Interdiscip. Top.* **2002**, *65*, 041806.

- (57) Rasmussen, K.; Kalosakas, G. Improved Numerical Algorithm for Exploring Block Copolymer Mesophases. *J. Polym. Sci., Part B: Polym. Phys.* **2002**, *40*, 1777–1783.
- (58) Xie, N.; Liu, M. J.; Deng, H. L.; Li, W. H.; Qiu, F.; Shi, A. C. Macromolecular Metallurgy of Binary Mesocrystals Via Designed Multiblock Terpolymers. *J. Am. Chem. Soc.* **2014**, *136*, 2974–2977.
- (59) Fredrickson, G. H. *The Equilibrium Theory of Inhomogeneous Polymers*; Oxford University Press on Demand, 2006.
- (60) Matsen, M. W.; Bates, F. S. Block Copolymer Microstructures in the Intermediate-Segregation Regime. *J. Chem. Phys.* **1997**, *106*, 2436–2448.
- (61) Stasiak, P.; Matsen, M. W. Efficiency of Pseudo-Spectral Algorithms with Anderson Mixing for the SCFT of Periodic Block-Copolymer Phases. *Eur. Phys. J. E: Soft Matter Biol. Phys.* **2011**, *34*, 110.
- (62) Thompson, R. B.; Rasmussen, K. O.; Lookman, T. Improved Convergence in Block Copolymer Self-Consistent Field Theory by Anderson Mixing. *J. Chem. Phys.* **2004**, *120*, 31–34.
- (63) Mogi, Y.; Kotsuji, H.; Kaneko, Y.; Mori, K.; Matsushita, Y.; Noda, I. Preparation and Morphology of Triblock Copolymers of the ABC Type. *Macromolecules* **1992**, *25*, 5408–5411.
- (64) Mogi, Y.; Mori, K.; Matsushita, Y.; Noda, I. Tricontinuous Morphology of Triblock Copolymers of the ABC Type. *Macromolecules* **1992**, *25*, 5412–5415.
- (65) Auschra, C.; Stadler, R. New Ordered Morphologies in ABC Triblock Copolymers. *Macromolecules* **1993**, *26*, 2171–2174.
- (66) Stadler, R.; Auschra, C.; Beckmann, J.; Krappe, U.; Voight-Martin, I.; Leibler, L. Morphology and Thermodynamics of Symmetric Poly(A-block-B-block-C) Triblock Copolymers. *Macromolecules* **1995**, *28*, 3080–3097.
- (67) Deng, H. L.; Li, W. H.; Qiu, F.; Shi, A. C. Self-Assembled Morphologies of Linear and Miktoarm Star Triblock Copolymer Monolayers. *J. Phys. Chem. B* **2017**, *121*, 4642–4649.
- (68) Breiner, U.; Krappe, U.; Stadler, R. Evolution of the “Knitting Pattern” Morphology in ABC Triblock Copolymers. *Macromol. Rapid Commun.* **1996**, *17*, 567–575.
- (69) Ott, H.; Abetz, V.; Altstadt, V. Morphological Studies of Poly(styrene)-block-poly(ethylene-co-butylene)-block-poly(methyl methacrylate) in the Composition Region of the “Knitting Pattern” Morphology. *Macromolecules* **2001**, *34*, 2121–2128.
- (70) The “wettability” analogy is thoughtfully recommended by the reviewer.